Topics in Catalysis (2022) 65:433–447
https://doi.org/10.1007/s11244-021-01534-w

ORIGINAL PAPER

Effect of Lewis Acids on the Catalyst Activity for Alkene Metathesis, *Z*-/*E*- Selectivity and Stability of Tungsten Oxo Alkylidenes

J. Haydée Merino[1] · Jesús Bernad[1] · Xavier Solans-Monfort[1]

Accepted: 9 November 2021 / Published online: 27 November 2021

Abstract
Lewis acids increase the catalytic activity of classical heterogeneous catalysts and molecular d^0 tungsten oxo alkylidenes in a variety of olefin metathesis processes. The formation of labile adducts between the metal complex and the Lewis acid has been observed experimentally and suggested to be involved in the catalyst activity increase. In this contribution, DFT (M06) calculations have been performed to determine the role of Lewis acids on catalyst activity, Z-/E- selectivity and stability by comparing three W(E)(CHR)(2,5-dimethylpyrrolide)(O-2,6-dimesithylphenoxide) (E = oxo, imido or oxo-Lewis acid adduct) alkylidenes. Results show that the formation of the alkylidene—Lewis acid adducts influences the reactivity of tungsten oxo alkylidenes due to both steric and electronic effects. The addition of the Lewis acid on the E group increases its bulkiness and this decreases catalyst *Z*-selectivity. Moreover, the interaction between the oxo ligand and the Lewis acid decreases the donating ability of the former toward the metal. This is important when the oxo group has either a ligand in trans or in the same plane that is competing for the same metal d orbitals. Therefore, the weakening of oxo donating ability facilitates the cycloaddition and cycloreversion steps and it stabilizes the productive trigonal bipyramid metallacyclobutane isomer. The two factors increase the catalytic activity of the complex. The electron donating tuneability by the coordination of the Lewis acid also applies to catalyst deactivation and particularly the key β-hydride elimination step. In this process, the transition states show a ligand in pseudo trans to the oxo. Therefore, the presence of the Lewis acid decreases the Gibbs energy barrier significantly. Overall, the optimization of the E group donating ability in each step of the reaction makes tungsten oxo alkylidenes more reactive and this applies both for the catalytic activity and catalyst deactivation.

Keywords Olefin metathesis · Density functional theory · Catalyst deactivation · Metal alkylidenes · Lewis acid

1 Introduction

Olefin metathesis is a key reaction in organic synthesis that implies the exchange of alkylidene substituents between alkenes. It has been applied to the synthesis of a large variety of molecules including raw materials, polymers, and drugs [1–8]. The reaction only takes place in presence of a catalyst. Silica and alumina supported molybdenum and tungsten oxides are within the first catalyst precursors and they have been applied in industrial applications util today [9]. The active species operating in these systems has not been characterized in detail, but they are thought to be metal oxo alkylidenes. Remarkably, addition of Lewis acids to these systems enhances their catalytic activity through a process that it is not well understood.

In 1971, Hérrison and Chauvin proposed the today's accepted reaction mechanism (Scheme 1) [2, 10]. It states that metal alkylidenes are the catalytic active species and metallacyclobutanes the key intermediates. Moreover, the catalytic cycle implies two olefin metathesis processes, each one composed of a cycloaddition and a cycloreversion step. The reaction mechanism proposed by Chauvin paved the way for the synthesis of metal alkylidenes. Some of the first active well-defined molecular catalysts were tungsten oxo alkylidenes and oxo alkyl complexes that act as precursors of the metal alkylidene (**1**–**4** in Scheme 2) [11–14]. These complexes are highly active towards olefin metathesis and their catalytic activity can usually be increased by adding Lewis acids in the media as in the case of classical heterogeneous catalysts. However, they deactivate fast and this, together with the development

✉ Xavier Solans-Monfort
Xavier.solans@uab.cat

[1] Departament de Química, Universitat Autònoma de Barcelona, 08193 Bellaterra, Spain

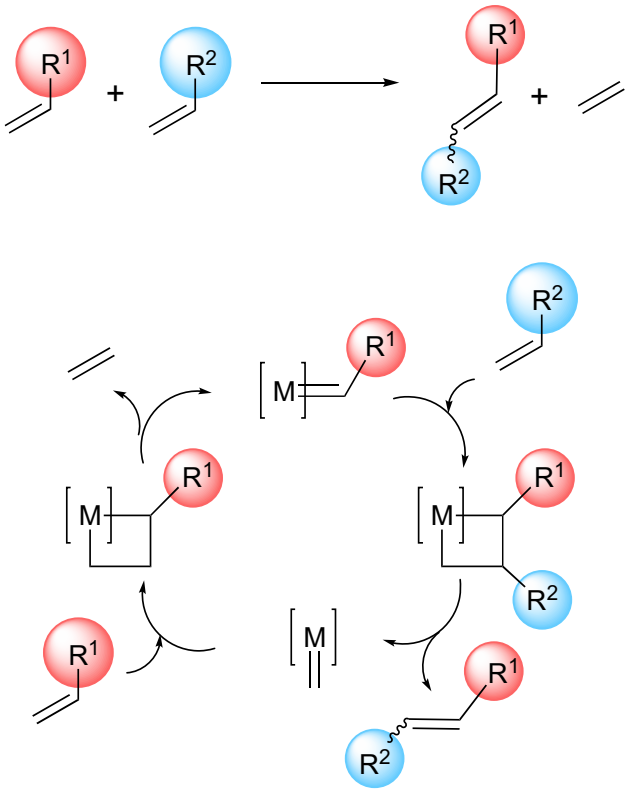

Scheme 1 Chauvin's mechanistic proposal

of d^0 imido alkylidene complexes ($\mathbf{5_{Mo}}$-$\mathbf{10_{Mo}}$and $\mathbf{5_W}$-$\mathbf{10_W}$) [15–25] as well as ruthenium carbenes (i.e. **11** and **12**) [26–34] prevented its further development since last decade.

In 2011, Schrock and co-workers reported the synthesis of a series of tungsten oxo alkylidenes bearing a pyrrolyl and a large alkoxy ancillary ligand (**13** and **14** in Scheme 2) [35]. These complexes are efficient and highly *Z*-selective olefin metathesis catalysts particularly on the homocoupling of terminal olefin and the ring opening metathesis polymerization (ROMP) of substituted norbornenes. In the subsequent years, the Schrock group reported other tungsten oxo alkylidenes and the role of ancillary ligands on the catalytic activity and product selectivity were deeply discussed (i.e. **15** and **16**) [36–42]. Moreover, Buchmeiser and co-workers synthetized a series of very active cationic tungsten oxo alkoxy alkylidene bearing an N-heterocyclic carbene (NHC) as fourth ligand (**17**–**18**) [43–45]. Both Schrock and Buchmeiser tungsten oxo alkylidenes were heterogenized by grafting on silica (**19**–**20**) [46–48]. Catalyst heterogenization prevented bimolecular deactivation and, as a consequence, the resulting complexes show very high catalytic activities and stabilities overperforming the imido analogues particularly when reacting with internal olefins. These high activities and stabilities are also reported for silica grafted

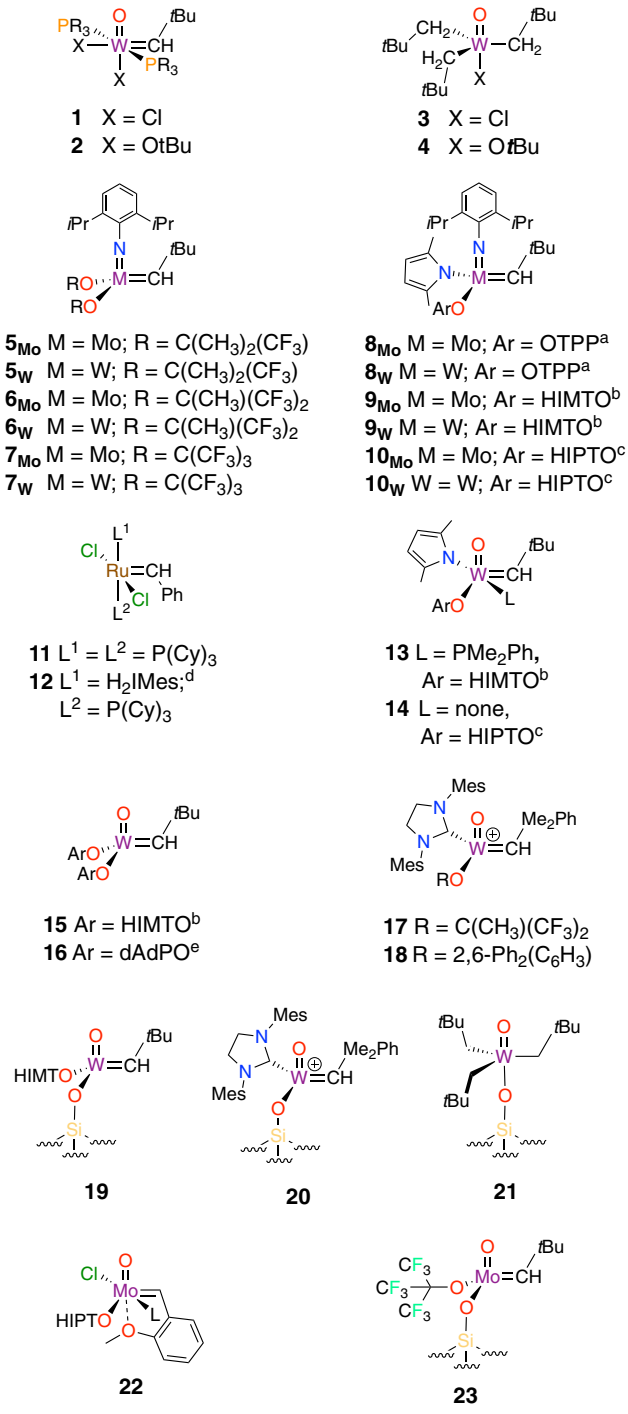

Scheme 2 Selected olefin metathesis catalysts and precursors. [a]OTPP = 2,3,5,6-$Ph_4(C_6H)$; [b]HIMTO = 2,6-$Mes_2(C_6H_3)$; [c]HIPTO = 2,6-(2,4,6-$iPr_3(C_6H_2)$)$_2(C_6H_3)$;[d]H_2IMes = 1,3-Mes_2-2-imidazolidinylidene; [e]dAdPO = 2,5-Ad_2-4-$CH_3(C_6H_2)$

tungsten oxo alkyl complexes that act as alkylidene precursors (**21** in Scheme 2) [49–51].

The knowledge acquired on tungsten oxo alkylidenes allowed the synthesis of molybdenum and vanadium oxo

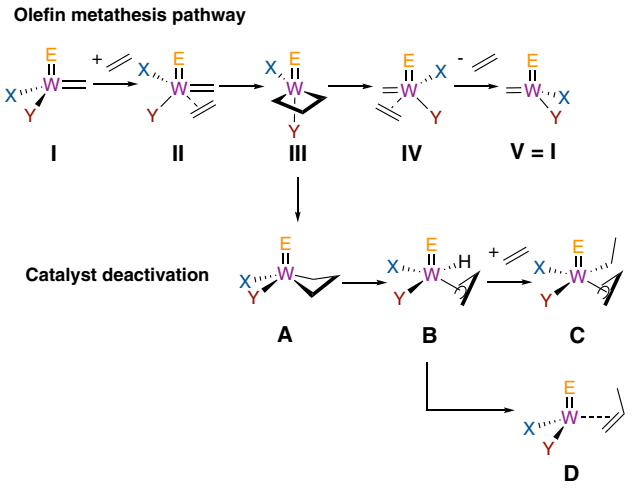

Scheme 3 Olefin metathesis and unimolecular catalyst deactivation reaction mechanisms

analogues as well as other molybdenum precursors that are also active in metathesis (**22, 23**) [40, 52–58]. The number of existing molybdenum oxo alkylidenes is limited and their activity for olefin metathesis is usually lower than that of tungsten species.

With the aim of bridging the gap between the activity of classical heterogeneous catalyst and the most recently reported well-defined molecular tungsten and molybdenum alkylidene, the effect of Lewis acids on the well-defined molecular complexes has been recently analyzed [35, 59]. Addition of $B(C_6F_5)_3$ as Lewis acid leads to the formation of a labile compound in which the Lewis acid is bonded to the oxo ligand (i.e. **13·B(C$_6$F$_5$)$_3$**). Moreover, an increase on the catalytic activity both towards terminal olefins and the ROMP of substituted norbornenes is usually observed. Remarkably, this activity increase is also commonly associated with a decrease of the *Z*-selectivity and more importantly catalyst stability. Analysis of the formed by-products shows the formation of propene and metallacyclopentene intermediates, suggesting that the deactivation occurs through β-hydride elimination and metal reduction without the reaction of additional ethene molecules as suggested for silica supported rhenium alkyl alkylidene alkylidyne complexes [60].

Theoretical studies on d^0 olefin metathesis have contributed to the understanding of the electronic structure of metal-alkylidenes and metallacyclobutane intermediates as well as the factors controlling catalyst activity and deactivation [60–71]. Today, it is well accepted that olefin coordination occurs trans to the strongest σ-donating ancillary ligand and the metallacyclobutane involved in the reaction pathway presents a trigonal bipyramid structure (TBP) with the doubly bond ligand (E) and the weakest σ-electron donor ligand in apical positions (Scheme 3 for the homocoupling reaction of ethene) [66, 68, 69]. This implies the inversion of the configuration of the stereogenic metal center [72]. Moreover, the square based metallacyclobutane isomer (SBP) is a resting state of the catalytic process which is involved in unimolecular deactivation through β-hydride elimination, a process taking place trans to the weakest σ-donating ligand [60, 68–70]. Since X and Y ligands play a different role, complexes with different X and Y ligands can show higher catalytic activities than species with X = Y. Strong σ-donor X ligands favor alkene coordination and imido (in comparison with oxo and alkylidyne E ligands) and weak σ-donor Y ligands stabilize the metallacyclobutane intermediate [60, 68–70]. The overall reactivity is a balance of these two effects. Catalyst stability with respect β-hydride elimination also depends on the nature of E, X and Y. β-hydride elimination is hampered when replacing alkyl as X ligand by pyrrolyl and the imido ligand by the stronger donor oxo group [60, 69, 70].

In this contribution, we perform DFT calculations to get electronic insights on the role of Lewis acids on the catalytic activity and *Z*-/*E*- selectivity of tungsten oxo alkylidenes as well as their stability toward unimolecular decomposition through β-hydride elimination. For that, we compared the reactivity, selectivity, and stability of three existing complexes bearing the same ancillary ligands except the doubly bonded (E) (**9$_W$**, **13** and **13·B(C$_6$F$_5$)$_3$** Scheme 2).

2 Computational Details

2.1 Level of Theory

All calculations are performed with the Minnesota M06 hybrid density functional [73, 74]. This functional has been shown to reproduce the experimental trends for systems where weak interactions are important and this includes the study of the olefin metathesis reaction [75–77]. Geometry optimizations are performed representing main group elements with the 6-31G(d,p) basis sets [78, 79]. Tungsten is represented with the small core Stuttgart pseudopotential together with the associated basis set enlarged with a f polarization function (α = 0.823) [80, 81]. The nature of the stationary points (minima or transition states) is verified by vibrational analysis. Moreover, IRC calculations are performed to determine the minima connected through **13·B(C$_6$F$_5$)$_3$-UU-TSII**, **13·B(C$_6$F$_5$)$_3$-UU-TSIII**, **13·B(C$_6$F$_5$)$_3$-TSAB**, **13·B(C$_6$F$_5$)$_3$-TSBC** and **13·B(C$_6$F$_5$)$_3$-TSBD**. We assume that for all other systems and orientations the connected minima are equivalent based on the geometrical similarities found within all transition states. The final energetics are obtained by single point calculations with the larger 6–311 + G(d,p) basis sets [82, 83] for main

group elements and the same representation of tungsten. In these single point calculations, solvent effects are included using the SMD continuum model [84] and toluene as solvent. Energies reported along the text are based on Gibbs energies ($G_{solv} = G_{gp} + \Delta G_{solv}$, where G_{gp} is the gas phase free energy and ΔG_{solv} stands for the solvation free energies) at 298.15 K and 1 atm. The thermal corrections are included at the smallest basis sets. All calculations are performed with the Gaussian09 package [85].

2.2 Model

The *Z*-/*E*- selectivity of tungsten oxo and imido olefin metathesis catalysts is analyzed by considering the 2-butene formation by reaction of propene with ethylidene of complexes $\mathbf{9_W}$, **13** and **13·BX$_3$** ($\mathbf{9_W}$**-I**, **13-I** and **13·BX$_3$-I**, respectively). In this context, the *Z*-/*E*- selectivity arises from the relative feasibilities of the four potential productive pathways (Scheme 4). This approach was used before with great success when studying the *Z*-/*E*- selectivity of ruthenium complexes [86]. The tungsten complexes are represented with the full bulk of the ancillary ligands (oxo or N-2,6*i*Pr-C_6H_3, 2,5-dimethylpyrrolyl and aryloxy ligands). The initial ethylidene species present two different isomers: *syn* with the methyl of ethylidene towards the oxo and *anti* with the methyl of the ethylidene away from the oxo and both are taken into account in the calculations. Moreover, two representations of the Lewis acid are considered: the experimentally used $B(C_6F_5)_3$ and BF_3 which mainly accounts for electronic effects.

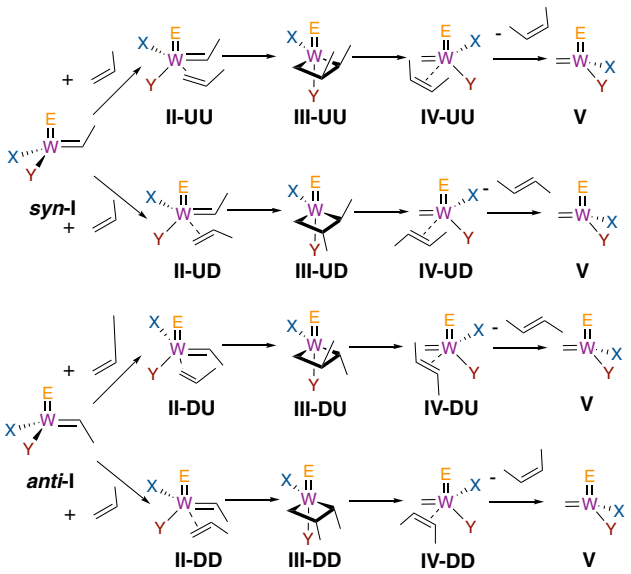

Scheme 4 Reaction pathways considered in this work

3 Results and Discussion

The aim of the present study is to give atomistic insights on the effect of Lewis acids on tungsten oxo alkylidenes' catalytic activity for olefin metathesis, their *Z*-/*E*- selectivity and their stability. For that, we compare the results obtained for **13-I** and $\mathbf{9_W}$**-I** ethylidene complexes as well as the oxo complex interacting with two Lewis acids $B(C_6F_5)_3$ (**13·B(C$_6$F$_5$)$_3$-I**) and BF_3 (**13·BF$_3$-I**), see Scheme 2. First, we focus on the structure of the oxo complexes with the aim of validating the computational approach with existing experimental data [35]. After that, we study the productive pathways for the propene conversion to *Z*- or *E*-2-butene catalyzed by **13-I**, $\mathbf{9_W}$**-I**, **13·B(C$_6$F$_5$)$_3$-I** or **13·BF$_3$-I**. Finally, we discuss catalyst stability towards β-hydride elimination [59, 60]. The nomenclature is constructed by three parts: the arabic number that indicates the catalyst precursor according to Scheme 2, a roman number or a capital letter that indicates the reaction intermediate following Scheme 4 (roman number for the productive process and the capital letter for the catalyst deactivation) and a combination of two U or D capital letters that indicate the orientation of the methyl groups of the alkylidene and reacting olefin. **U** indicates that the methyl points towards the E group and **D** that the methyl points towards the aryloxy ligand. The first letter refers to the substituent of the initial alkylidene while the latter refers to the methyl group of propene (Scheme 4).

3.1 Methodology Validation

The interaction of a Lewis acid with tungsten oxo alkylidenes is labile according to experiments [35]. Thus, we decided to evaluate the ability of the methodology used to reproduce experimental data of complexes **13** and **14** (Scheme 2) and particularly the following three observations [35]: (i) the synthesis of complex **13** leads to a pentacoordinated with a coordinated phosphine as fifth ligand; (ii) the addition of two equivalents of $B(C_6F_5)_3$ in a solution containing **13** leads to the formation of the **13·B(C$_6$F$_5$)$_3$** adduct in which the Lewis acid is labile: and (iii) Substitution of 2,6-dimesithylphenoxide (HIMTO) ligand by the bulkier O-2,6-(2,4,6-*i*PrC_6H_2)$_2$$C_6H_3$ (HIPTO) ligand allows the isolation of tetracoordinated *syn*-W(O)(CHtBu)(2,5-Me$_2$Pyr) (HIPTO) complex (**14**). Table 1 compares the computed and X-Ray diffraction determined geometry parameters and Fig. 1 shows a detailed view of the optimized structures computed for **13**, **14** and related adducts.

The ***syn*-13$_{\mathbf{No\text{-}PMe2Ph}}$** alkylidene presents a distorted tetrahedral coordination around tungsten with a short W=O (1.696 Å). The O=W=C angle is 105.0° and the W=C–H angle suggests the presence of an α–CH agostic interaction [65]. The *anti* isomer presents the same metal

Table 1 DFT (X-ray) geometry parameters (distances in Å and angles in degrees) for ***syn*-13**, ***syn*-13·B(C_6F_5)$_3$** and ***syn*-14**

	***syn*-13**	***syn*-13·B(C_6F_5)$_3$**	***syn*-14**
W=O	1.716(1.717)	1.757(1.759)	1.697(1.695)
W=C_{ene}	1.894 (1.900)	1.876(1.868)	1.887(1.886)
W–N_{Pyr}	2.062(2.074)	1.985(1.968)	2.011(2.001)
W–O_{Ar}	1.984(1.964)	1.870(1.860)	1.893(1.868)
W–P	2.667(2.580)		
O–B		1.536(1.571)	
W=C_{ene}–C_β	140.7(141.0)	142.3(155.4)	135.4(136.7)
W–O_{Ar}–C_{Ar}	156.8(159.8)	166.3(150.9)	165.1(166.9)
W–O–B		169.4	
P–W–N_{Pyr}	153.9		

coordination without the α–CH agostic interaction and it is less stable by 6.8 kcal mol^{-1}. Coordination of PMe_2Ph to ***syn*-13$_{No\text{-}PMe2Ph}$** is favorable by -1.5 kcal mol^{-1} and the resulting complex (***syn*-13**) presents a trigonal bipyramid coordination around tungsten with apical phosphine and pyrrolyl ligands. The computed W-L distance are close to the X-Ray values (Table 1). Remarkably, the ***anti*-13** is less stable by 10.6 kcal mol^{-1}, thus suggesting that phosphine coordination is less favorable in ***anti*-13$_{No\text{-}PMe2Ph}$**. Addition of $B(C_6F_5)_3$ forms ***syn*-13·B(C_6F_5)$_3$** in which the Lewis acid interacts with the oxo group. The B···O distance is 1.532 Å and this lengthens the W = O bond to 1.759 Å. The ***syn*-13·B(C_6F_5)$_3$** is -1.1 kcal mol^{-1} lower in Gibbs energy than ***syn*-13$_{No\text{-}PMe2Ph}$**, in agreement with the characterization of ***syn*-13·B(C_6F_5)$_3$** and the labile behavior of $B(C_6F_5)_3$ in solution.

Regarding complex **14**, calculations suggest that the substitution of the HIMTO ligand by the bulkier HIPTO stabilizes the *syn*- isomer with respect to the *anti*- one (Fig. 1). Moreover, they indicate that the largest bulkiness of the metal complex makes the coordination of PMe_2Ph unfavorable by about + 4.3/ + 4.4 kcal mol^{-1} and this is consistent with the isolation of the tetracoordinated complex of ***syn*-14**.

Overall, calculations on the precursors show that the methodology used in this work reproduces the structure of these complexes as well as the associated energetics. Particularly, calculations predict: i) the largest stability for the *syn*- isomer; ii) the marginally favorable phosphine coordination to **13$_{No\text{-}PMe2Ph}$** but the unfavorable phosphine coordination to **14**; and iii) the weak interaction between $B(C_6F_5)_3$ and the oxo group.

3.2 Effect of Lewis Acids on Catalyst Activity

The role of Lewis acids on the catalytic activity for olefin metathesis of tungsten oxo alkylidene complexes is discussed by comparing the propene metathesis with the ethylidene complexes **13-I**, **9$_W$-I**, **13·B(C_6F_5)$_3$-I** and **13·(BF_3)$_3$-I**. Table 2 summarizes the relative Gibbs energies with respect to separated reactants **N-I-U** + propene following the labelling of Schemes 2 and 4 and the relative reaction rates with respect to the UU route. The optimized structures can be found in the Supplementary Information.

The propene metathesis occurs through today's accepted reaction mechanism that involves the formation of an olefin complex, a cycloaddition step that leads to a metallacyclobutane intermediate with a trigonal pyramid structure and the reverse cycloreversion and olefin decoordination steps [60, 68–70]. Moreover, the square based metallacyclobutane isomer is a resting state of the reaction. Remarkably, we could not locate the transition state associated to olefin coordination and olefin decoordination. This is indicative that the barrier likely arises from the entropic term and thus can not be located by exploring the potential energy surface. This was highlighted in previous contributions [87, 88] and is particularly relevant when dispersion forces are taken into account at least partially.

The computed energy barriers with the tungsten oxo ethylidene **13-I** show that all steps are easy (within 1.5 and 10.1 kcal mol^{-1}) and thus all intermediates and transition states lie at energies that are accessible at reaction conditions. The highest in Gibbs energy structure is **13-TSIII-DD** and it lies 24.4 kcal mol^{-1} over **13-I-U** and propene. As found in model calculations [70], the reactive TBP metallacycle is significantly higher in energy than the SBP isomer (between 7.5 and 12.4 kcal mol^{-1}) and this is rationalized by the strong trans effect of the oxo ligand, which presents a very short W = O distance (1.71 Å). Overall, the lowest intermediate is separated reactants except for the **UD** pathway, where the SBP metallacycle (**13-A-UD**) is slightly lower in energy (-2.2 kcal mol^{-1}). The highest in Gibbs energy transition state is in all cases the cycloreversion step (**13-TSIII**), thus the energy span of the reaction is defined as the energy difference between **13-A-UD** and the cycloreversion transition state (**13-TSIII**) and it varies between 17.1 and 26.7 kcal mol^{-1}.

The energetics for the same processes catalyzed with tungsten imido alkylidene (**9$_W$-I**) present several similarities with the reactivity of **13-I** as well as remarkable differences. As for **13-I**, the highest in energy transition state is that associated to the cycloreversion (**9$_W$-TSIII**), while the global minimum is **9$_W$-III-UU**. Moreover, the computed energy spans are similar to those computed for **13-I** albeit marginally higher (between 18.1 and 25.6 kcal mol^{-1}). In contrast, the relative stability between TBP and SBP metallacyclobutane (**III** *vs.* **A**) isomers is inversed. That is, the reactive TBP isomer is more stable than the SBP resting state for the imido complex by 0.8–10.3 kcal mol^{-1}. This indicates that most of the initial catalyst remains on the productive pathway, and it does not accumulate on an isomer

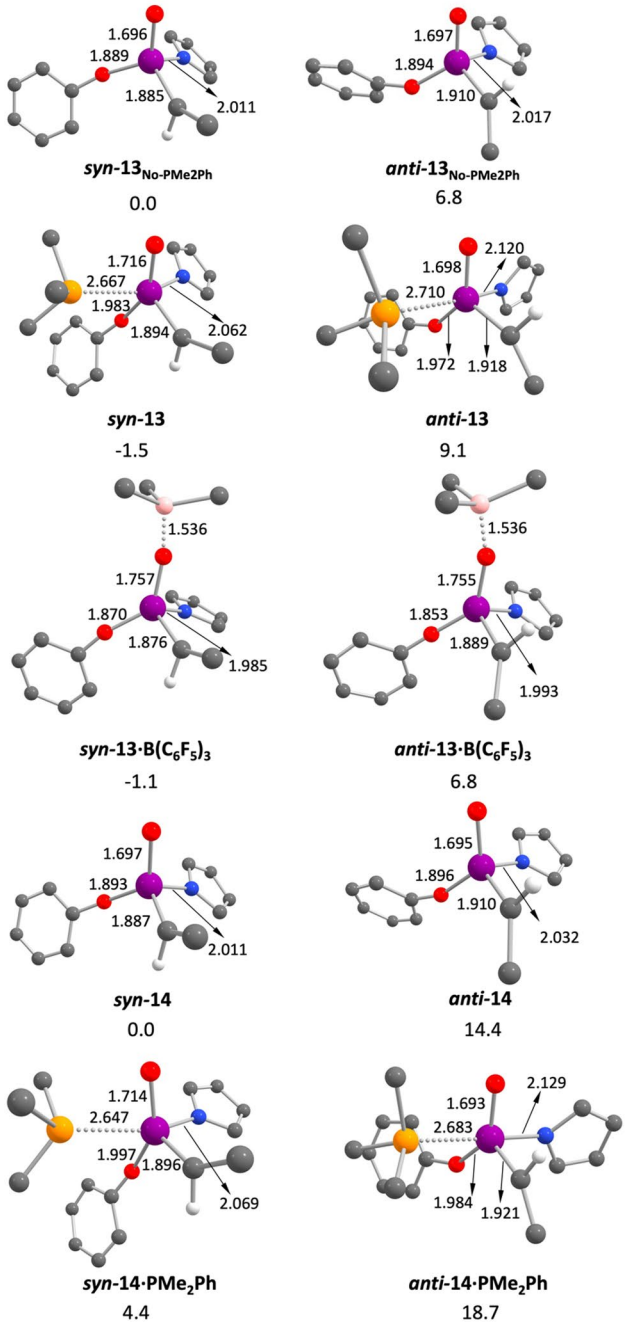

Fig. 1 Detailed view of the optimized structures for *syn*- and *anti*- **13** and **14** alkylidenes and related adducts as well as the relative energies (in kcal mol^{-1}) with respect to the ML_4 species ***syn*-13$_{No\text{-}PMe2Ph}$** or **14** and either PMe_2Ph or $B(C_6F_5)_3$

not involved in the olefin metathesis process. The stabilization of **III** can be rationalized by the lower trans effect of the imido ligand with respect to the oxo group, while the destabilization of **A** is likely due to steric repulsion between the large aryloxy and imido ligands. Overall, the small difference in the energy spans of **9_W-I** and **13-I** and the different relative stabilities of the metallacyclobutane isomers suggest that the two complexes should present similar reactivities in absence of catalyst deactivation.

The presence of $B(C_6F_5)_3$ as Lewis acid leads to the formation of **13·B(C_6F_5)$_3$-I** in which $B(C_6F_5)_3$ is weakly interacting with the oxo group through a O-B bond of 1.571 Å. The formation of the ***syn*-13·B(C_6F_5)$_3$-I** adduct is exergonic by -1.9 kcal mol^{-1} (-3.7 kcal mol^{-1} for the *anti*- isomer) and the O-$B(C_6F_5)_3$ produces a weakening of the W = O bond (W = O distance elongation of about 0.05 Å), as in the case of the catalyst precursor. The reaction of **13·B(C_6F_5)$_3$-I** with propene shows that the formation of **13·B(C_6F_5)$_3$** adduct is in general marginally exergonic for all intermediates and transition states with respect to the analogous structures of **13** and $B(C_6F_5)_3$. The main exception is the SBP metallacyclobutane intermediate. In this case, although we find the adduct as a minimum of the potential energy surfaces, calculations predict that the Lewis acid–metal complex formation is unfavorable by 2.7–6.4 kcal mol^{-1}. The larger stabilization due to the presence of the Lewis acid is observed for the cycloreversion transition state. Consequently, the energy span defined by the difference between separated reactants (the global minimum of the reaction) and the transition state for either cycloaddition (**TSII**) or cycloreversion (**TSIII**) decreases significantly and becomes between 13.3 and 19.7 kcal mol^{-1} and, this agrees with the higher catalytic activity of tungsten oxo alkylidenes in presence of Lewis acids.

With the aim of isolating the steric and electronic effects we considered BF_3 as a smaller model of Lewis acid. Results for **13·BF_3-I** are equivalent to those obtained with **13·B(C_6F_5)$_3$**: (i) the formation of the adduct for all intermediates and transition states involved in the productive process is exergonic with respect to the analogues structures and separated BF_3; (ii) The BF_3-oxo interaction weakens the W=O bond; (iii) the BF_3-oxo group interaction is unfavorable for the SBP isomer; and (iv) the energy span decreases significantly, thus indicating that the presence of the Lewis acid increases the catalyst activity. Consequently, the effect of the Lewis acid has mainly an electronic contribution that is stronger at the cycloaddition and cycloreversion transition states as well as the at the TBP metallacyclobutane isomer but not on the SBP one. Remarkably, these are the species in which the oxo ligand has either a ligand in *trans* or the oxo group is in the same plane of the alkylidene and aryloxy ligands. This suggest that the higher catalytic activity of tungsten oxo alkylidenes in presence of a Lewis acid can be mainly attributed to two factors: i) the decrease of the electron donating ability of the oxo group, thus the *trans* influence of the oxo ligand and ii) and increase of the electrophilicity of the metal center when the **N·BX_3** adduct is formed as evidenced by the Natural Population Charges of tungsten in the initial ethylidene species (q_{13} = 1.39, $q_{13\cdot B(C6F5)3}$ = 1.63 and $q_{13\cdot BF3}$ = 1.51). The higher metal electrophilicity favors

Table 2 Relative Gibbs energies with respect to ***syn*-N-I** and propene (in kcal mol^{-1}) of all intermediates and transition states associated with propene homocoupling reaction leading to either *E*- and *Z*-2-butene

Complex	Path	I	TSI	II	TSII	III	TSIV	IV	TSIV	V	A	k_{AA}/k_{UU}[a]
13-I	**UU (*Z*-)**[a]	0.0	–	8.4	10.5	7.6	14.8	10.9	–	1.2	0.1	1.0
	UD (*E*-)[a]	0.0	–	12.2	15.0	8.1	18.0	14.0	–	0.3	− 2.3	$4.5{\cdot}10^{-3}$
	DU (*E*-)[a]	3.4	–	12.1	13.9	10.4	20.5	14.4	–	0.3	2.2	$6.6{\cdot}10^{-6}$
	DD (*Z*-)[a]	3.4	–	16.0	17.5	15.4	24.4	11.9	–	1.2	3.0	$9.1{\cdot}10^{-8}$
9_W-I	**UU (*Z*-)**[a]	0.0	–	–	–	− 2.2	16.6	12.7	–	2.3	8.1	1.0
	UD (*E*-)[a]	0.0	–	–	–	2.8	18.1	17.3	–	1.4	3.6	$6.7{\cdot}10^{-2}$
	DU (*E*-)[a]	2.2	–	–	–	7.1	23.4	19.1	–	1.4	9.2	$8.7{\cdot}10^{-6}$
	DD (*Z*-)[a]	2.2	–	–	–	4.7	23.1	20.5	–	2.3	8.8	$1.4{\cdot}10^{-5}$
13·B(C_6F_5)$_3$-I	**UU (*Z*-)**[a]	0.0 (− 1.9)	–	10.9 (0.6)	13.3 (0.9)	10.0 (0.4)	11.6 (− 5.2)	7.1 (− 5.7)	–	1.0 (− 2.1)	8.5 (6.4)	1.0
	UD (*E*-)[a]	0.0 (− 1.9)	–	9.6 (− 4.5)	15.6 (− 1.3)	0.7 (− 9.3)	11.5 (− 8.4)	10.7 (− 5.2)	–	0.1 (− 2.1)	2.3 (2.7)	$2.1{\cdot}10^{-2}$
	DU (*E*-)[a]	1.7 (− 3.7)	–	11.9 (− 2.2)	13.4 (− 2.5)	7.7 (− 4.7)	19.7 (− 2.7)	13.8 (− 2.6)	–	0.1 (− 2.1)	8.5 (4.4)	$2.0{\cdot}10^{-5}$
	DD (*Z*-)[a]	1.7 (− 3.7)	–	10.2(− 7.7)	16.0(− 3.4)	11.1 (− 6.2)	16.7 (− 9.6)	7.1 (− 6.7)	–	1.0 (− 2.1)	8.3 (3.4)	$3.2{\cdot}10^{-3}$
13·BF_3-I	**UU (*Z*-)**[a]	0.0 (0.9)	–	− 0.6 (− 8.1)	3.1 (− 6.5)	− 0.7 (− 7.5)	9.7 (− 4.2)	4.8 (− 5.2)	–	4.3 (4.0)	3.4	1.0
	UD (*E*-)[a]	0.0 (0.9)	–	4.7 (− 6.6)	4.8 (− 9.3)	− 1.0 (− 8.2)	10.5 (− 6.6)	8.0 (− 5.1)	–	3.3 (4.0)	0.5	0.26
	DU (*E*-)[a]	3.4 (0.9)	–	6.6 (− 4.6)	9.8 (− 3.2)	1.2 (− 8.3)	10.7 (− 8.9)	8.8(− 4.7)	–	3.3 (4.0)	7.6	0.18
	DD (*Z*-)[a]	3.4	–	8.7 (− 6.4)	10.2 (− 6.4)	4.9 (− 9.6)	14.8 (− 8.6)	11.7 (0.7)	–	4.3 (4.0)	7.0	$1.8{\cdot}10^{-4}$

[a] Relative rate with respect to the UU pathway computed using the energy span model, assuming the global minima as the common most stable intermediate: $\frac{K_{AA}}{K_{UU}} = e^{-\left[\left(\delta G_{AA} - \delta G_{UU}\right)/RT\right]}$

the olefin coordination, while the decrease of the *trans* effect of the oxo ligand stabilizes the TBP metallacyclobutane intermediate and the cycloaddition and cycloreversion transition states. Overall, the Lewis acid allows adapting the electron donating ability of the oxo ligand in each step of the reaction and this leads to a smoother Gibbs energy profile.

3.3 Effect of Lewis Acids on Catalyst Z-/E-Selectivity

The analysis of the *Z*-/*E*- selectivity of each catalyst implies comparing the relative Gibbs energies and rates of the most favorable pathway leading to *Z*-2-butene and that of the most favorable pathway leading to *E*-2-butene (Table 2). For that, we first focus on how the Gibbs energies of each intermediate and transition state varies as function of the position of the methyl groups and then we discuss the energetics, in terms of energy span, of the different pathways.

The relative stability of the olefin metathesis intermediates involved in the productive process (**I**, **II**, **III** and **IV**) and the transition states connecting them (**TSII** and **TSIII**) for all considered complexes **13-I**, $\mathbf{9_W}$**-I**, **13·B(C$_6$F$_5$)$_3$** and **13·BF$_3$** follow the same general trend with very few exceptions. In general, **UU** is the most stable isomer and **DD** the highest in energy species in each stationary point. The detailed order is **UU** < **UD** < **DU** < **DD**. The few exceptions are mainly associated with those species presenting the bulkier E ligands (imido or the O–B(C$_6$F$_5$)$_3$). In the **UU** pathway the two substituents point toward the E group and in the case of the less favorable **DD** route, the substituents points toward the aryloxy ligand. Therefore, the relative stability of the different routes is mainly controlled by the ligand bulkiness. That is, since the E group is generally smaller than the aryloxy ligand, the preferred relative orientation shows the two methyl groups pointing to E, the two pathways presenting one methyl towards E and the other towards the bulky aryloxy ligand have intermediate energies and the route with the two methyls pointing toward the aryloxy ligand is the less favorable one.

The relative stabilities of the SBP metallacyclobutane resting state do not follow the same order. The SBP metallacyclebutane stability trend follows: **UD** > **UU** ~ **DD** > **DU**. The puckered form of the metallacyclebutane fragment leads to the presence of equatorial and axial sites. Thus, the structure with the two methyl groups in equatorial (**A-UD**) is lower in Gibbs energy than the structures with one methyl in axial position (**A-DD** and **A-UU**), and **A-DU**, with the two substituents in axial posions, is usually the less stable one. Overall, the relative stabilities of the SBP isomer are controlled by the local structure of the metallacyclobutane fragment and not by the bulkiness of the ligands. Consequently, the relative stabilities of the different reactant-alkylidene orientation in the SBP metallacyclobutane isomer are not sensitive to the alkylidene ancillary ligands. However, this relative stabilities of the SBP metallacyclobutane species does not have any effect on defining the *Z*-/*E*- selectivity, since according to the energy span model this essentially originates from the relative stabilities of the transition state for cycloreversion.

Overall, the *Z*-/*E*- selectivity is defined by the relative Gibbs energies of **N-TSIII-UU** and **N-TSIII-UD**, except for **13·B(C$_6$F$_5$)$_3$**, which is defined by the relative Gibbs energies between **13·B(C$_6$F$_5$)$_3$-TSII-UU** and **13·B(C$_6$F$_5$)$_3$-TSII-UD.** For the case, of **13-I** with a very small oxo ligand as E, the energy difference is large (3.1 kcal mol^{-1}), thus suggesting a > 99% selectivity for the *Z*-product at least at the initial stages of the reaction (the rate of the UD pathway is $4.5 \cdot 10^{-3}$ times slower than that of the UU route). The Gibbs energy difference between the same transition states of the tungsten imido ethylidene analogue ($\mathbf{9_W}$**-I**) is smaller (1.7 kcal mol^{-1}) suggesting a smaller selectivity that is related to the bulkiness increase of the E group (the ratio between k_{UD} and k_{UU} is $6.7 \cdot 10^{-2}$). Interestingly, the preference for the **UU** pathway is also small for **13·BF$_3$-I** ($\Delta\delta G = 0.8$ kcal mol^{-1} and $k_{UD}/k_{UU} = 0.26$) and **13·B(C$_6$F$_5$)3-I**, thus explaining the loss in Z-selectivity when adding a Lewis acid in the reaction mixture.

Analysis of **TSIII** transition state geometries (Fig. 2) give further support to the importance of the ligand bulkiness. When going from **13** to **13·BF$_3$** and **13·B(C$_6$F$_5$)$_3$**, there is a general increase of E group size in all directions due to tetrahedral environment around boron. This implies an opening of the W···C$_{ole}$-C$_{CH3}$ angle in the **UU-TSIII** pathway only (Fig. 2) and a significant variation of the dihedral angle defined by the reacting carbon atoms. These two facts indicates that the released olefin orientation in the **UU** route is influenced by the bulk of E in the larger systems, preventing the achievement of the optimal structure in $\mathbf{9_W}$, **13·BF$_3$** and **13·B(C$_6$F$_5$)$_3$**. Moreover, comparison between the **UU** and **DD** pathways as limit cases, indicates that the W–O-C$_{aryloxy}$ angle associated to the Y ligand increases when substituents point toward Y. This suggests that the Y ligand also adapts to avoid repulsive interactions with the methyl groups of the releasing olefin. Consequently, **TSIII** is destabilized in the **UD**, **DU** and **DD** routes. In summary, despite the reported values could be sensitive to the conformational exploration, the computed data indicate that the interaction between the Lewis acid and the oxo group makes the resulting adduct to have a large E ligand that decreases the preference for the *Z*- product. In this way, the use of smaller Lewis acids or alternatively small Y ligands that could favor the DD route may eventually increase the catalyst activity and retain a larger amount of *Z*- selectivity.

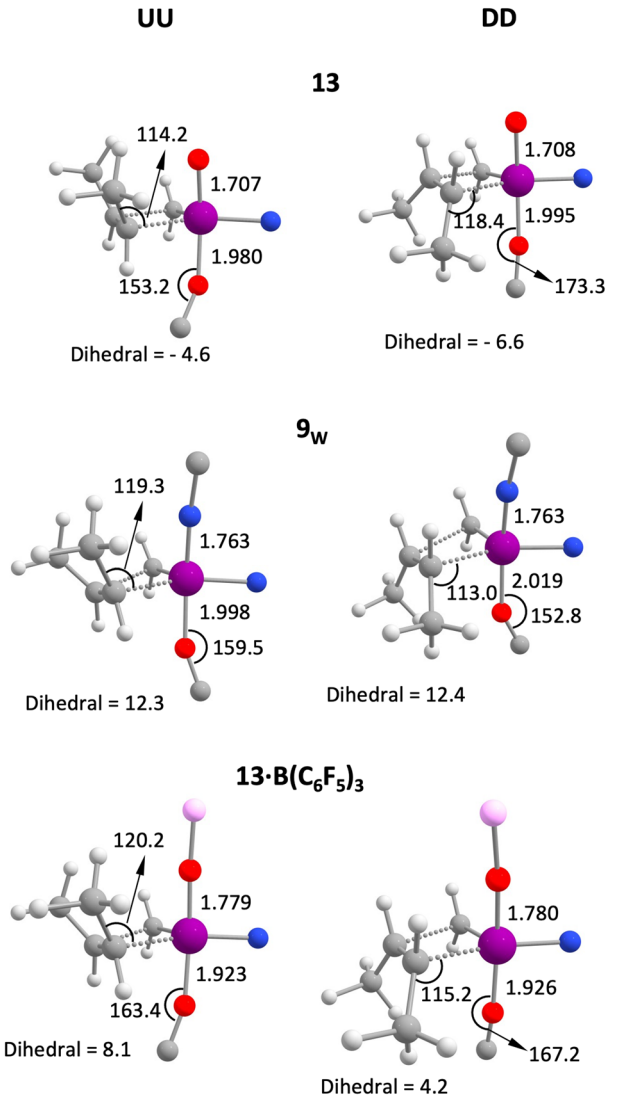

Fig. 2 Detailed view of the metal coordination of the optimized structures for the UU and DD cycloreversion transition states (TSIII) for **13**, $\mathbf{9_W}$ and $\mathbf{13{\cdot}B(C_6F_5)_3}$. Distances are in Å and angles in degrees. The reported dihedral corresponds to that defined by the C_{ole}–C_{ole}–W–C_{ene} atoms

3.4 Effect of Lewis Acids on Catalyst Deactivation

Based on the species formed after olefin metathesis, two main catalyst deactivation pathways for d^0 alkylidenes have been reported in the literature: (i) bimolecular coupling of two alkylidenes [89] and (ii) β-hydride elimination from the unsubstituted SBP metallacyclobutane (**A**) [59, 60, 90]. While the former does not seem to be favored by the presence of Lewis acids (it may even disfavor it due to the ligand bulkiness increase), the addition of Lewis acid leads to the formation of a W(IV) olefin complex compatible with the β-hydride elimination at **A**.[59] Here, we studied deactivation through β-hydride elimination of the methylidene complexes of **13**, $\mathbf{9_W}$ and $\mathbf{13{\cdot}B(C_6F_5)_3}$ catalysts. We considered two different final products: the W(IV) olefin complex (**D**) and the alkyl allyl complex (**C**) resulting from ethene addition to the allyl hydride intermediate (**B**), which has been proposed to be the first step for side product formation and other catalyst deactivation processes [60]. Results for catalyst deactivation are summarized in Fig. 3 (the nomenclature is based on that used in Schemes 2 and 3) and Table 3 reports the energetics for the degenerate metathesis of ethene for comparison.

The Gibbs energies associated to the ethene metathesis with methylidene follows the same trends described before and particularly, the addition of $B(C_6F_5)_3$ favors the cycloaddition step and stabilizes the TBP metallacyclobutane (**III**) intermediate with respect to the SBP (**A**) one. When comparing with the propene metathesis with the ethylidene complex, one observes that most of the intermediates and transition states are stabilized with respect to separated reactants as a consequence of reducing the reactant bulkiness. Therefore, the nature of the olefin and alkylidene substituents tunes the energetics but does not modify the previously described trends.

The deactivation of **13** starts with the β-hydride elimination. This step takes place with the hydride being transferred trans to the weakest σ-donating aryloxy ligand. The computed Gibbs energy barrier is high (35.0 kcal mol^{-1}), thus suggesting a large stability of **13** if bimolecular coupling does not occur. The resulting allyl hydride intermediate (**B**) is 15.3 kcal mol^{-1} higher in energy than the SBP metallacycle (**A**) thus, it must further evolve to achieve catalyst deactivation. The ethene insertion to the metal hydride presents an even higher in Gibbs energy transition state (42.7 kcal mol^{-1} with respect to methylidene + ethene). This indicates that despite the process is thermodynamically favorable ($\Delta G^{\circ}_{298} = -$ 12.0 kcal mol^{-1}) ethene insertion is a rare event. In contrast, the reductive coupling between the hydride and the allyl ligands that leads to the formation a W(IV) olefin complex is largely favored thermodynamically ($\Delta G^{\circ}_{298} = -$ 27.4 kcal mol^{-1}) and the associated energy barrier is low ($\Delta G^{\ddagger\circ}_{298} = 4.7$ kcal mol^{-1}). Indeed, the transition state for the reductive coupling is located 29.4 kcal mol^{-1} lower in Gibbs energy than the transition state for ethene insertion, indicating that the most likely deactivation process for **13** is the formation of a W(IV) olefin complex and the highest in Gibbs energy transition state is that associated with the β-hydride process. This is in contradiction with the DFT results reported for silica grafted (OSi)Re(C*t*Bu)(CH*t*Bu)(CH_2*t*Bu) [60], but this could be either related to the modeling strategy or to the different reactivity of the two complex as suggested by the experimentally observed side products in each case [59, 60].

Substitution of the oxo group by an imido ligand makes the β-hydride elimination and the alkene insertion easier.

The Gibbs energies with respect to separated reactants of the associated transition states are 25.4 and 40.2 kcal mol^{-1} for the β-hydride and the ethene insertion respectively. Again, ethene insertion appears as an unlikely process, thus suggesting that another process should take place. In this context, reductive coupling leading to **D** is thermodynamically favorable ($\Delta G^{\circ}_{298} = -15.4$ kcal mol^{-1}) and the associated Gibbs energy barrier lower than that of the ethene insertion (30.5 vs. 40.2 kcal mol^{-1}). Noteworthily, the transition state for the reductive coupling is higher in Gibbs energy than that of the β-hydride elimination. Therefore, $\mathbf{9_W}$ decomposition through β-hydride elimination leads to also to a W(IV) olefin complex, but, in contrast to **13**, the highest in Gibbs energy transition state is that associated with the formation of the olefin complex. Overall, deactivation of $\mathbf{9_W}$ is easier than the deactivation of **13**.

The $\mathbf{13{\cdot}B(C_6F_5)_3}$ adducts associated to the deactivation of **13** in presence of a Lewis acid are minima of the potential energy surfaces. The species are especially favorable for the allyl hydride intermediate (**B**) and the transition states associated to the β-hydride elimination (**TSAB**) and ethene insertion (**TSBC**) (values in parenthesis in Fig. 3). Consequently, both the β-hydride elimination from $\mathbf{13{\cdot}B(C_6F_5)_3}$**-A** and the ethene insertion to $\mathbf{13{\cdot}B(C_6F_5)_3}$**-B** are easier than the analogous processes without the presence of the Lewis acid. The relative Gibbs energies of $\mathbf{13{\cdot}B(C_6F_5)_3}$**-TSAB** and $\mathbf{13{\cdot}B(C_6F_5)_3}$**-TSBC** with respect to separated $\mathbf{13{\cdot}B(C_6F_5)}$**-V** and ethene are 31.3 and 36.6 kcal mol^{-1}, thus ethene insertion is more challenging than the β-hydride. The Gibbs energy barrier for the reductive coupling leading to **D** is 20.2 kcal mol^{-1} and, although the process is more challenging than in absence of the Lewis acid, it is still largely more accessible than the ethene insertion. Therefore, similarly to $\mathbf{9_W}$ and **13**, the $\mathbf{13{\cdot}B(C_6F_5)_3}$ intramolecular deactivation leads to a W(IV) olefin complex, and it involves two steps, β-hydride elimination and the reductive coupling between the allyl and hydride ligands. The transition state for the β-hydride is the highest transition state in the catalyst deactivation process, indicating a mechanistic difference between the oxo complexes (rate determining step is the β-hydride elimination) and the imido alkylidene (the highest in energy step is the reductive coupling). The comparison of the relative Gibbs energies of the highest transition states with respect to separated species indicate that $\mathbf{13{\cdot}B(C_6F_5)_3}$ is more prone to deactivate through a unimolecular process than **13**.

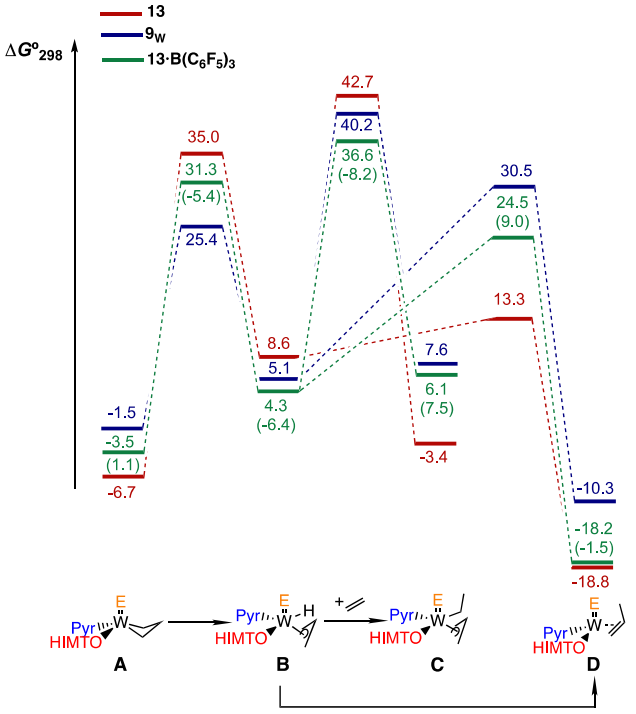

Fig. 3 Gibbs energy profile (in kcal mol^{-1}) for the unimolecular deactivation through β-hydride elimination at the SBP metallacycle. Values in parenthesis correspond to the interaction energy between the metal complex and the Lewis acid

Trends between the three complexes for the relative Gibbs energies of **TSAB**, **TSBC** and **TSBD** can be rationalized in terms of the donating ability of the E ligand. As shown in Fig. 4, both the β-hydride elimination and the alkene insertion imply the presence of a ligand in (pseudo)-trans to the E group. In the case of the β-hydride elimination transition state, one of the C_α carbons of the metallacycle is in pseudo trans to E (Fig. 4). On the other hand, ethene insertion takes place in the vacant site trans to the E and the transition state presents a short W···C_{ene} (between 2.44 and 2.51 Å (Fig. 4). Consequently, in both cases the transition state stability is penalized when the E group is a strong donating group (i.e. oxo). Moreover, the two processes become easier when the donating ability of E becomes weaker, which is achieved either by replacing the oxo for an imido ligand or by adding a Lewis that tunes the electron density of the oxo group.

The relative stabilities of the transition states for the reductive coupling of **13**, $\mathbf{9_W}$ and $\mathbf{13{\cdot}B(C_6F_5)_3}$ are inversed with respect to **TSAB** and **TSBC** and a strong donating E

Table 3 Gibbs energies (in kcal mol^{-1}) of all intermediates and transition states associated with ethene metathesis reaction

Catalyst	V	TSI	II	TSII	III	A
13	0.0	–	9.0	10.9	− 0.3	− 6.7
$13{\cdot}B(C_6F_5)_3$	0.0	–	6.1	9.2	− 3.9	− 3.5

See Schemes 3 and 4 for labelling

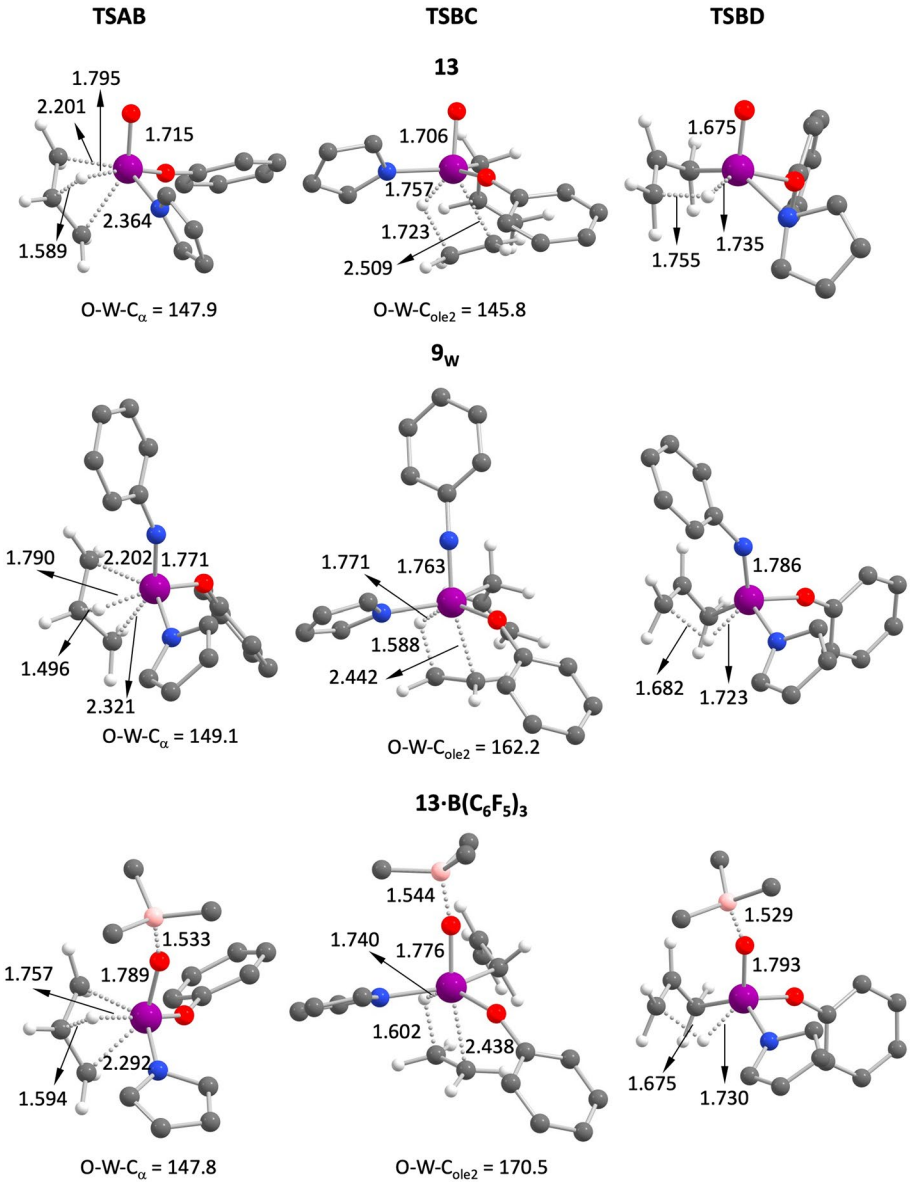

Fig. 4 Detailed view of the optimized structures for TSAB, TSBC and TSBD for **13**, $\mathbf{9_W}$ and $\mathbf{13{\cdot}B(C_6F_5)_3}$ complexes. Distances in Å angles in degrees

ligand favors the process. In this case, part of the metal-hydride bond is loss in the **TSBD** transition state when compared with the allyl hydride and thus the presence of strong donating ligands better compensate the loss in electron density on the metal center. This is particularly the case of the tungsten oxo complex **13**, which presents a low energy barrier, while the opposite extreme is represented by the imido complex $\mathbf{9_W}$.

4 Conclusions

DFT (M06) calculations have been performed to rationalize the effect of Lewis acids on the catalytic activity for olefin metathesis, *Z-*/*E-* selectivity and catalyst stability of tungsten oxo alkylidene complexes. For that, we compared three W(E)(CHR)(2,5-dimethylpyrrolide)(2,6-mesithylphenoxide) complexes differing only on the nature of the doubly bonded E group: oxo, imido and an oxo group interacting with a Lewis acid. Results show that the formation of a stable oxo-Lewis acid adduct occurs mainly when the metal is tetra-coordinated and more significantly when the E group has another ligand in trans or in the same plane competing for the same empty metal d orbitals. This is particularly the case of the cycloaddition and cycloreversion transition states, the productive TBP metallacycle isomer and the transition state for β-hydride elimination, which is the highest in energy transition state associated to the unimolecular deactivation of tungsten oxo alkylidene complexes. In these adducts, the resulting E group is bulky due to the presence of the phenyl rings of the $B(C_6F_5)_3$ Lewis acid and the ligand steric hindrance is comparable to that of the large aryloxy ligand.

Therefore, the *Z*-/*E*- selectivity, defined by the Gibbs energy difference between the lowest transition state leading to the *Z*- and *E*- product, decreases significantly. Moreover, the Lewis acid has also an electronic influence. The oxo-Lewis acid interaction decreases the oxo electron donating ability, which decreases its trans influence and makes the metal slightly more electrophilic. Consequently, the cycloaddition and cycloreversion Gibbs energy barriers with respect to separated reactants are lowered and the TBP metallacyclobutane isomer, which is much higher in Gibbs energy than the SBP metallacycle resting state for the oxo complex, is stabilized. The two factors lead to an increase of catalyst activity in presence of the Lewis acid, thus rationalizing the experimental observations. Unfortunately, the tuneability of the oxo electron donating ability also affects the transition state for the β-hydride elimination, the rate determining transition state in the catalyst deactivation. Since the H-transfer implies the presence of the C_α carbon of the original metallacycle fragment pseudo trans to the E group, the decrease of the trans influence of the oxo group by the interaction with a Lewis acid stabilizes the transition state and favors catalyst deactivation when the Lewis acid—oxo adduct is formed.

Overall, the presence of Lewis acid in the reacting media allows adapting the electron donating ability of the oxo ligand in each step of the reaction. This takes place by forming a Lews acid—oxo alkylidene adduct when a weak electron donor E group is needed and by the decoordination of the Lewis acid when a strong electron donating E group stabilizes one intermediate or transition state. This makes the oxo alkylidene more reactive both for catalyzing the olefin metathesis reaction and in those processes involving catalyst deactivation. Therefore, the optimal use of Lewis acids requires a subtle balance between the catalytic activity increase and the alkylidene stability loss. Despite present conclusions are obtained for a reduced series of molecular tungsten oxo alkylidenes, similar effects of the Lewis acid are expected for other metal oxo complexes, and they could also be envisaged in classical heterogeneous catalysts.

Supplementary Information The online version contains supplementary material available at https://doi.org/10.1007/s11244-021-01534-w.

Acknowledgements Financial support from the Ministerio de Ciencia e Innovación (PID2020-112715GB-I00) and the Generalitat de Catalunya (2017SGR1323) is acknowledged. XSM is grateful for the Professor Agregat Serra Húnter position.

Funding Open Access Funding provided by Universitat Autonoma de Barcelona. Ministerio de Ciencia e Innovación—Grant: PID2020-112715 GB-I00 and Generalitat de Catalunya—Grant: 2017SGR1323.

Data Availability The Cartesian Coordinates of all optimized structures can be found as an xyz and pdf files in the Supplementary Information.

Declarations

Conflict of interest Authors declare no conflict of interest.

References

1. Calderon N, Chen HY, Scott KW (1967) Olefin metathesis—a novel reaction for skeletal transformations of unsaturated hydrocarbons. Tetrahedron Lett 34:3327–3329
2. Chauvin Y (2006) Olefin metathesis: the early days (Nobel lecture). Angew Chem Int Ed 45:3740–3747. https://doi.org/10.1002/anie.200601234
3. Grubbs RH (2006) Olefin-metathesis catalysts for the preparation of molecules and materials (Nobel lecture). Angew Chem Int Ed 45:3760–3765. https://doi.org/10.1002/anie.200600680
4. Schrock RR (2006) Multiple metal-carbon bonds for catalytic metathesis reactions (Nobel lecture). Angew Chem Int Ed 45:3748–3759. https://doi.org/10.1002/anie.200600085
5. Samojłowicz C, Bieniek M, Grela K (2009) Ruthenium-based olefin metathesis catalysts bearing N-heterocyclic carbene ligands. Chem Rev 109:3708–3742. https://doi.org/10.1021/cr800524f
6. Ogba OM, Warner NC, O'Leary DJ, Grubbs RH (2018) Recent advances in ruthenium-based olefin metathesis. Chem Soc Rev 47:4510–4544. https://doi.org/10.1039/c8cs00027a
7. Copéret C, Berkson ZJ, Chan KW et al (2021) Olefin metathesis: what have we learned about homogeneous and heterogeneous catalysts from surface organometallic chemistry? Chem Sci 12:3092–3115. https://doi.org/10.1039/d0sc06880b
8. Hoveyda AH, Liu Z, Qin C et al (2020) Impact of ethylene on efficiency and stereocontrol in olefin metathesis: when to add it, when to remove it, and when to avoid it. Angew Chem Int Ed 59:22324–22348. https://doi.org/10.1002/anie.202010205
9. Mol J (2004) Industrial applications of olefin metathesis. J Mol Catal A 213:39–45. https://doi.org/10.1016/j.molcata.2003.10.049
10. Hérisson J-L, Chauvin Y (1970) Catalyse de transformation des oléines par les complexes du tungstene. Die Makromol Chem 141:161–176
11. Wengrovius JH, Schrock RR, Churchill MR et al (1980) Tungsten-oxo alkylidene complexes as olefin metathesis catalysts and the crystal structure of W(O)(CHCMe3)PEt3)Cl2. J Am Chem Soc 309:4515–4516
12. Kress JRM, Russell MJM, Wesolek MG, Osborn JA (1980) Tungsten(VI) and molybdenum(VI) oxo-alkyl species. Their role in the metathesis of olefins. J Chem Soc Chem Commun 2:431–432. https://doi.org/10.1039/C39800000431
13. Kress J, Wesolek M, le Ny JP, Osborn JA (1981) Molecular complexes for efficient metathesis of olefins. The oxo-ligand as a catalyst-cocatalyst bridge and the nature of the active species.

J Chem Soc Chem Commun. https://doi.org/10.1039/C39810001039
14. Wengrovius JH, Schrock RR (1982) Synthesis and characterization of tungsten oxo neopentylidene complexes. Organometallics 1:148–155. https://doi.org/10.1021/om00061a026
15. Murdzek JS, Schrock RR, Complexes A, Ar M (1987) Well-characterized olefin metathesis catalysts that contain molybdenum. Organometallics 6:1373–1374
16. Schrock RR, DePue RT, Feldman J et al (1988) Preparation and reactivity of several alkylidene complexes of the type W(CHR') (N-2, 6–C6H3-i-Pr2)(OR)2 and related tungstacyclobutane complexes. controlling metathesis activity through the choice of alkoxide ligand. J Am Chem Soc 110:1423–1435. https://doi.org/10.1021/ja00213a014
17. Schrock RR, Murdzek JS, Bazan GC et al (1990) Synthesis of molybdenum imido alkylidene complexes and some reactions involving acyclic olefins. J Am Chem Soc 112:3875–3886. https://doi.org/10.1021/ja00166a023
18. Bazan GC, Oskam JH, Cho H et al (1991) Living ring-opening metathesis polymerization of. 2,3-difunctionalized 7-oxanorbornene and 7-oxanorbornadienes by Mo(CHCMe2R)(N-2,6–C_6H_3-i-Pr_2)(O-t-Bu)$_2$ and Mo(CHCMe$_2$R)(N-2,6–C_6H_3-i-Pr_2)(OCMe$_2$CF$_3$)$_2$. J Am Chem Soc 113:6899–6907
19. Schrock RR (2009) Recent advances in high oxidation state Mo and W imido alkylidene chemistry. Chem Rev 109:3211–3226. https://doi.org/10.1021/cr800502p
20. Townsend EM, Schrock RR, Hoveyda AH (2012) Z-selective metathesis homocoupling of 1,3-dienes by molybdenum and tungsten monoaryloxide pyrrolide (MAP) complexes. J Am Chem Soc 134:11334–11337. https://doi.org/10.1021/ja303220j
21. Jiang AJ, Zhao Y, Schrock RR, Hoveyda AH (2009) Highly Z-selective metathesis homocoupling of terminal olefins. J Am Chem Soc 131:16630–16631. https://doi.org/10.1021/ja908098t
22. Wang C, Yu M, Kyle AF et al (2013) Efficient and selective formation of macrocyclic disubstituted Z alkenes by ring-closing metathesis (RCM) reactions catalyzed by Mo- or W-based monoaryloxide pyrrolide (MAP) complexes: applications to total syntheses of epilachnene, yuzu lactone, ambrettolide, Epothilone C, and Nakadomarin A Chem. Eur J 19:2726–2740. https://doi.org/10.1002/chem.201204045
23. Meek SJ, Obrien, Llaveria J RV et al (2011) Catalytic Z-selective olefin cross-metathesis for natural product synthesis. Nature 471:461–466. https://doi.org/10.1038/nature09957
24. Flook MM, Jiang AJ, Schrock RR et al (2009) Z-selective olefin metathesis processes catalyzed by a molybdenum hexaisopropylterphenoxide monopyrrolide complex. J Am Chem Soc 131:7962–7963. https://doi.org/10.1021/ja902738u
25. Jiang AJ, Simpson JH, Müller P, Schrock RR (2009) Fundamental studies of tungsten alkylidene imido monoalkoxidepyrrolide complexes. J Am Chem Soc 131:7770–7780. https://doi.org/10.1021/ja9012694
26. Schwab P, Grubbs RH, Ziller JW (1996) Synthesis and applications of RuCl2(=CHR′)(PR3)2: the influence of the alkylidene moiety on metathesis activity. J Am Chem Soc 118:100–108. https://doi.org/10.1021/ja952676d
27. Nguyen ST, Johnson LK, Grubbs RH, Ziller JW (1992) Ring-opening metathesis polymerization (ROMP) of norbornene by a Group VIII carbene complex in protic media. J Am Chem Soc 114:3974–3975. https://doi.org/10.1021/ja00036a053
28. Scholl M, Ding S, Lee CW, Grubbs RH (1999) Synthesis and activity of a new generation of ruthenium-based olefin metathesis catalysts coordinated with 1,3-dimesityl-4,5-dihydroimidazol-2-ylidene ligands. Org Lett 1:953–956. https://doi.org/10.1021/ol990909q
29. Kingsbury JS, Harrity JPA, Bonitatebus PJ, Hoveyda AH (1999) A recyclable Ru-based metathesis catalyst. J Am Chem Soc 121:791–799. https://doi.org/10.1021/ja983222u
30. Garber SB, Kingsbury JS, Gray BL, Hoveyda AH (2000) Efficient and recyclable monomeric and dendritic Ru-based metathesis catalysts. J Am Chem Soc 122:8168–8179. https://doi.org/10.1021/ja001179g
31. Michrowska A, Bujok R, Harutyunyan S et al (2004) Nitro-substituted Hoveyda-Grubbs ruthenium carbenes: enhancement of catalyst activity through electronic activation. J Am Chem Soc 126:9318–9325. https://doi.org/10.1021/ja048794v
32. Keitz BK, Endo K, Herbert MB, Grubbs RH (2011) Z -selective homodimerization of terminal olefins with a ruthenium metathesis catalyst. J Am Chem Soc 133:9686–9688. https://doi.org/10.1021/ja203488e
33. Keitz BK, Endo K, Patel PR et al (2012) Improved ruthenium catalysts for Z-selective olefin metathesis. J Am Chem Soc 134:693–699. https://doi.org/10.1021/ja210225e
34. Khan RKM, Torker S, Hoveyda AH (2013) Readily accessible and easily modifiable Ru-based catalysts for efficient and Z-selective ring-opening metathesis polymerization and ring-opening/cross- metathesis. J Am Chem Soc 135:10258–10261. https://doi.org/10.1021/ja404208a
35. Peryshkov DV, Schrock RR, Takase MK et al (2011) Z-selective olefin metathesis reactions promoted by tungsten Oxo alkylidene complexes. J Am Chem Soc 133:20754–20757. https://doi.org/10.1021/ja210349m
36. Peryshkov DV, Schrock RR (2012) Synthesis of tungsten oxo alkylidene complexes. Organometallics 31:7278–7286. https://doi.org/10.1021/om3008579
37. Forrest WP, Axtell JC, Schrock RR (2014) Tungsten oxo alkylidene complexes as initiators for the stereoregular polymerization of 2,3-dicarbomethoxynorbornadiene. Organometallics 33:2313–2325. https://doi.org/10.1021/om5002364
38. Forrest WP, Weis JG, John JM et al (2014) Stereospecific ring-opening metathesis polymerization of norbornadienes employing tungsten oxo alkylidene initiators. J Am Chem Soc 136:10910–10913. https://doi.org/10.1021/ja506446n
39. Townsend EM, Hyvl J, Forrest WP et al (2014) Synthesis of molybdenum and tungsten alkylidene complexes that contain sterically demanding arenethiolate ligands. Organometallics 33:5334–5341. https://doi.org/10.1021/om500655n
40. Boudjelel M, Zhai F, Schrock RR et al (2021) Oxo 2-adamantylidene complexes of Mo(VI) and W(VI). Organometallics 40:838–842. https://doi.org/10.1021/acs.organomet.1c00086
41. Yan T, Venkatramani S, Schrock RR, Müller P (2019) Synthesis of tungsten oxo alkylidene biphenolate complexes and ring-opening metathesis polymerization of norbornenes and norbornadienes. Organometallics 38:3144–3150. https://doi.org/10.1021/acs.organomet.9b00377
42. Kruger AG, Brucks SD, Yan T et al (2021) Stereochemical control yields mucin mimetic polymers. ACS Central Sci 7:624–630. https://doi.org/10.1021/acscentsci.0c01569
43. Buchmeiser MR (2018) Molybdenum imido, tungsten imido and tungsten oxo alkylidene N-heterocyclic carbene olefin metathesis catalysts. Chem Eur J 24:14295–14301. https://doi.org/10.1002/chem.201802497
44. Schowner R, Frey W, Buchmeiser MR (2015) Cationic tungsten-oxo-alkylidene-N-heterocyclic carbene complexes: highly active olefin metathesis catalysts. J Am Chem Soc 137:6188–6191. https://doi.org/10.1021/jacs.5b03788
45. Hauser PM, Musso, Frey W, Buchmeiser MR JV (2021) Cationic tungsten oxo alkylidene N-heterocyclic carbene complexes via hydrolysis of cationic alkylidyne progenitors. Organometallics 40:927–937. https://doi.org/10.1021/acs.organomet.1c00035

46. Conley MP, Mougel V, Peryshkov DV et al (2013) A well-defined silica-supported tungsten oxo alkylidene is a highly active alkene metathesis catalyst. J Am Chem Soc 135:19068–19070. https://doi.org/10.1021/ja410052u
47. Pucino M, Mougel V, Schowner R et al (2016) Cationic silica-supported N-heterocyclic carbene tungsten oxo alkylidene sites: highly active and stable catalysts for olefin metathesis. Angew Chem Int Ed 55:4300–4302. https://doi.org/10.1002/anie.201510678
48. Conley MP, Forrest WP, Mougel V et al (2014) Bulky aryloxide ligand stabilizes a heterogeneous metathesis catalyst. Angew Chem Int Ed 53:14221–14224. https://doi.org/10.1002/anie.201408880
49. Mazoyer E, Merle N, de Mallmann A et al (2010) Development of the first well-defined tungsten oxo alkyl derivatives supported on silica by SOMC: towards a model of WO_3/SiO_2 olefin metathesis catalyst. Chem Commun 46:8944–8946. https://doi.org/10.1039/c0cc02507k
50. Bouhoute Y, Garron A, Grekov D et al (2014) Well-defined supported mononuclear tungsten oxo species as olefin metathesis pre-catalysts. ACS Catal 4:4232–4241. https://doi.org/10.1021/cs501294j
51. Qureshi ZS, Hamieh A, Barman S et al (2017) SOMC-designed silica supported tungsten Oxo imidazolin-2-iminato methyl pre-catalyst for olefin metathesis reactions. Inorg Chem 56:861–871. https://doi.org/10.1021/acs.inorgchem.6b02424
52. Bukhryakov KV, Schrock RR, Hoveyda AH et al (2018) Syntheses of molybdenum oxo alkylidene complexes through addition of water to an alkylidyne complex. J Am Chem Soc 140:2797–2800. https://doi.org/10.1021/jacs.8b00499
53. Zhai F, Bukhryakov KV, Schrock RR et al (2018) Syntheses of molybdenum oxo benzylidene complexes. J Am Chem Soc 140:13609–13613. https://doi.org/10.1021/jacs.8b09616
54. de Jesus SJ, Pucino M, Zhai F et al (2021) Boosting the metathesis activity of molybdenum oxo alkylidenes by tuning the anionic ligand σ donation. Inorg Chem 60:6875–6880. https://doi.org/10.1021/acs.inorgchem.0c03173
55. Pucino M, Zhai F, Gordon CP et al (2019) Silica-supported molybdenum oxo alkylidenes: bridging the gap between internal and terminal olefin metathesis. Angew Chem Int Ed 58:11816–11819. https://doi.org/10.1002/anie.201903325
56. Merle N, le Quéméner F, Barman S et al (2017) Well-defined silica supported bipodal molybdenum oxo alkyl complexes: a model of the active sites of industrial olefin metathesis catalysts. Chem Commun 53:11338–11341. https://doi.org/10.1039/c7cc06041f
57. Merle N, le Quéméner F, Bouhoute Y et al (2017) Well-defined molybdenum oxo alkyl complex supported on silica by surface organometallic chemistry: a highly active olefin metathesis pre-catalyst. J Am Chem Soc 139:2144–2147. https://doi.org/10.1021/jacs.6b11220
58. Belov DS, Fenoll DA, Chakraborty I, et al (2021) Synthesis of vanadium oxo alkylidene complex and its reactivity in ring-closing olefin metathesis reactions. Organometallics acs.organomet.1c00425. https://doi.org/10.1021/acs.organomet.1c00425
59. Peryshkov DV, Forrest WP, Schrock RR et al (2013) B(C6F5)3 activation of oxo tungsten complexes that are relevant to olefin metathesis. Organometallics 32:5256–5259. https://doi.org/10.1021/om4007906
60. Leduc A-M, Salameh A, Soulivong D et al (2008) beta-h transfer from the metallacyclobutane: a key step in the deactivation and byproduct formation for the well-defined silica-supported rhenium alkylidene alkene metathesis catalyst. J Am Chem Soc 130:6288–6297. https://doi.org/10.1021/ja800189a
61. Rappé AK, Goddard WA (1982) Olefin metathesis. a mechanistic study of high-valent group 6 catalysts. J Am Chem Soc 162:448–456
62. Folga E, Ziegler T (1993) Density functional study on molybdacyclobutane and its role in olefin metathesis. Organometallics 12:325–337. https://doi.org/10.1021/om00026a018
63. Wu YD, Peng ZH (1997) Theoretical studies on alkene addition to molybdenum alkylidenes. J Am Chem Soc 119:8043–8049. https://doi.org/10.1021/ja970644f
64. Goumans TPM, Ehlers AW, Lammertsma K (2005) The asymmetric Schrock olefin metathesis catalyst. A Comput Study Organometal 24:3200–3206. https://doi.org/10.1021/om0501091
65. Solans-Monfort X, Clot E, Copéret C, Eisenstein O (2005) Understanding structural and dynamic properties of well-defined rhenium-based olefin metathesis catalysts, Re(=CR)(=CHR)(X)(Y), from DFT and QM/MM calculations. Organometallics 24:1586–1597. https://doi.org/10.1021/om048997s
66. Solans-Monfort X, Clot E, Copéret C, Eisenstein O (2005) d(0) Re-based olefin metathesis catalysts, Re(=CR)(=CHR)(X)(Y): The key role of X and Y ligands for efficient active sites. J Am Chem Soc 127:14015–14025. https://doi.org/10.1021/ja053528i
67. Herz K, Podewitz M, Stöhr L et al (2019) Mechanism of olefin metathesis with neutral and cationic molybdenum imido alkylidene N-hetercyclic carbene complexes. J Am Chem Soc 141:8264–8276. https://doi.org/10.1021/jacs.9b02092
68. Poater A, Solans-Monfort X, Clot E et al (2007) Understanding d(0)-olefin metathesis catalysts: which metal, which ligands? J Am Chem Soc 129(8207):8216. https://doi.org/10.1021/ja070625y
69. Solans-Monfort X, Copéret C, Eisenstein O (2010) Shutting down secondary reaction pathways: the essential role of the pyrrolyl ligand in improving silica supported d(0)-ML4 alkene metathesis catalysts from DFT calculations. J Am Chem Soc 132:7750–7757. https://doi.org/10.1021/ja101597s
70. Solans-Monfort X, Copéret C, Eisenstein O (2012) Oxo vs imido alkylidene d(0)-metal species: how and why do they differ in structure, activity, and efficiency in alkene metathesis? Organometallics 31:6812–6822. https://doi.org/10.1021/om300576r
71. Solans-Monfort X, Copéret C, Eisenstein O (2015) Metallacyclobutanes from Schrock-type d(0) metal alkylidene catalysts: structural preferences and consequences in alkene metathesis. Organometallics 34(1668):1680. https://doi.org/10.1021/acs.organomet5b00147
72. Meek SJ, Malcolmson SJ, Li B et al (2009) The significance of degenerate processes to enantioselective olefin metathesis reactions promoted by stereogenic-at-Mo complexes. J Am Chem Soc 131:16407–16409. https://doi.org/10.1021/ja907805f
73. Zhao Y, Truhlar DG (2008) The M06 suite of density functionals for main group thermochemistry, thermochemical kinetics, noncovalent interactions, excited states, and transition elements: two new functionals and systematic testing of four M06-class functionals and 12 other functionals Theor. Chem Acc 120:215–241. https://doi.org/10.1007/s00214-007-0310-x
74. Zhao Y, Truhlar DG (2008) Density functionals with broad applicability in chemistry. Acc Chem Res 41:157–167. https://doi.org/10.1021/ar700111a
75. Zhao Y, Truhlar DG (2007) Attractive noncovalent interactions in the mechanism of Grubbs second-generation Ru catalysts for olefin metathesis. Org Lett 9:1967–1970. https://doi.org/10.1021/ol0705548
76. Minenkov Y, Occhipinti G, Jensen VR (2009) Metal−phosphine bond strengths of the transition metals: a challenge for DFT. J Phys Chem A 113:11833–11844. https://doi.org/10.1021/jp902940c
77. Paredes-Gil K, Solans-Monfort X, Rodriguez-Santiago L et al (2014) DFT study on the relative stabilities of substituted

Ruthenacyclobutane intermediates involved in olefin cross-metathesis reactions and their interconversion pathways. Organometallics 33:6065–6075. https://doi.org/10.1021/om500718a
78. Hehre WJ, Ditchfield R, Pople JA (1972) Self—consistent molecular orbital methods. XII. Further extensions of Gaussian—type basis sets for use in molecular orbital studies of organic molecules. J Chem Phys 56:2257–2261. https://doi.org/10.1063/1.1677527
79. Francl MM, Pietro WJ, Hehre WJ et al (1982) Self-consistent molecular orbital methods. XXIII. A polarization-type basis set for second-row elements. J Chem Phys 77:3654–3665. https://doi.org/10.1063/1.444267
80. Andrae D, Häussermann U, Dolg M et al (1990) Energy-adjusted ab initio pseudopotentials for the second and third row transition elements. Theor Chimica Acta 77:123–141. https://doi.org/10.1007/BF01114537
81. Ehlers AW, Böhme M, Dapprich S et al (1993) A set of f-polarization functions for pseudo-potential basis sets of the transition metals Sc-Cu, Y-Ag and La-Au. Chem Phys Lett 208:111–114. https://doi.org/10.1016/0009-2614(93)80086
82. Hariharan PC, Pople JA (1973) The influence of polarization functions on molecular orbital hydrogenation energies. Theor Chimica Acta 28:213–222. https://doi.org/10.1007/BF00533485
83. Frisch MJ, Pople JA, Binkley JS (1984) Self-consistent molecular orbital methods 25. Supplementary functions for Gaussian basis sets. J Chem Phys 80:3265–3269. https://doi.org/10.1063/1.447079
84. Marenich AV, Cramer CJ, Truhlar DG (2009) Universal solvation model based on solute electron density and on a continuum model of the solvent defined by the bulk dielectric constant and atomic surface tensions. J Phys Chem B 113:6378–6396. https://doi.org/10.1021/jp810292n
85. Frisch MJ, Trucks GW, Schlegel HB, et al (2009) Gaussian09, Revision D.01
86. Liu P, Xu X, Dong X et al (2012) Z -selectivity in olefin metathesis with chelated Ru catalysts: computational studies of mechanism and selectivity. J Am Chem Soc 134:1464–1467. https://doi.org/10.1021/ja2108728
87. Solans-Monfort X (2014) DFT study on the reaction mechanism of the ring closing enyne metathesis (RCEYM) catalyzed by molybdenum alkylidene complexes. Dalton Trans 43:4573–4586. https://doi.org/10.1039/c3dt53242a
88. Kesharwani MK, Elser I, Musso JV et al (2020) Reaction mechanism of ring-closing metathesis with a cationic molybdenum imido alkylidene N-heterocyclic carbene catalyst. Organometallics 39:3146–3159. https://doi.org/10.1021/acs.organomet.0c00311
89. Lopez LPH, Schrock RR (2004) Formation of dimers that contain unbridged W(IV)/W(IV) double bonds. J Am Chem Soc 126:9526–9527. https://doi.org/10.1021/ja0400988
90. Tsang WCP, Hultzsch KC, Alexander JB et al (2003) Alkylidene and metalacyclic complexes of tungsten that contain a chiral biphenoxide ligand. synthesis, asymmetric ring-closing metathesis, and mechanistic investigations. J Am Chem Soc 125:2652–2666. https://doi.org/10.1021/ja0210603